

"Seeing" electroencephalogram through the skull: imaging prefrontal cortex with fast optical signal

Andrei V. Medvedev

Georgetown University Medical Center
Center for Functional and Molecular Imaging
Washington, DC 20057

Jana M. Kainerstorfer

University of Vienna
Department of Physics
Vienna, Austria
and
Eunice Kennedy Shriver National Institute of Child Health
and Human Development
National Institutes of Health Section on Analytical and
Functional Biophotonics
Program on Pediatric Imaging and Tissue Sciences
Bethesda, Maryland 20892

Sergey V. Borisov*

Georgetown University Medical Center
Center for Functional and Molecular Imaging
Washington, DC 20057

Amir H. Gandjbakhche

Eunice Kennedy Shriver National Institute of Child Health
and Human Development
National Institutes of Health Section on Analytical and
Functional Biophotonics
Program on Pediatric Imaging and Tissue Sciences
Bethesda, Maryland 20892

John VanMeter

Georgetown University Medical Center
Center for Functional and Molecular Imaging
Washington, DC 20057

1 Introduction

In 1945, it was discovered that neuronal activity causes changes in the optical properties of nervous tissue.¹ Later, changes in the optical properties of brain cells have been demonstrated by many research groups using brain slices^{2,3} and intact cortical tissue.^{4,5} Since then, optical methods have been widely used to explore brain function, utilizing contrast agents (extrinsic signal) or measuring light detected from a source (e.g., laser diode) propagating through the tissue (intrinsic signal). In addition, several research groups have demonstrated that optical methods can be used to measure hemodynamic responses through the skull in human subjects, and these findings led to the development of near-infrared spectroscopy (NIRS) as a new noninvasive imaging tool.^{6–10} Due to the fact that the major absorber of near-infrared light in biological tissue is hemoglobin,

Abstract. Near-infrared spectroscopy is a novel imaging technique potentially sensitive to both brain hemodynamics (slow signal) and neuronal activity (fast optical signal, FOS). The big challenge of measuring FOS noninvasively lies in the presumably low signal-to-noise ratio. Thus, detectability of the FOS has been controversially discussed. We present reliable detection of FOS from 11 individuals concurrently with electroencephalogram (EEG) during a Go-NoGo task. Probes were placed bilaterally over prefrontal cortex. Independent component analysis (ICA) was used for artifact removal. Correlation coefficient in the best correlated FOS–EEG ICA pairs was highly significant ($p < 10^{-8}$), and event-related optical signal (EROS) was found in all subjects. Several EROS components were similar to the event-related potential (ERP) components. The most robust "optical N200" at $t = 225$ ms coincided with the N200 ERP; both signals showed significant difference between targets and nontargets, and their timing correlated with subject's reaction time. Correlation between FOS and EEG even in single trials provides further evidence that at least some FOS components "reflect" electrical brain processes directly. The data provide evidence for the early involvement of prefrontal cortex in rapid object recognition. EROS is highly localized and can provide cost-effective imaging tools for cortical mapping of cognitive processes. © 2010 Society of Photo-Optical Instrumentation Engineers. [DOI: 10.1117/1.3505007]

Keywords: near-infrared spectroscopy; fast optical signal; event-related signal; electroencephalogram; independent component analysis; visual object detection.

Paper 10102SS received Feb. 27, 2010; accepted for publication Apr. 16, 2010; published online Nov. 23, 2010.

NIRS methodology measures a signal dependent on blood oxygenation, which is similar to the blood oxygenation level dependent (BOLD) signal measured by functional magnetic resonance imaging (fMRI). Neurovascular mechanisms are relatively slow, and a hemodynamic optical signal usually includes both an increase in concentration of oxygenated hemoglobin and a decrease in deoxygenated hemoglobin, which develop within a few seconds and peak at 5 to 10 s after the stimulus/task onset, as has been demonstrated in many studies using various functional tasks.^{11–14} In contrast, an optical signal that depends on changes in optical properties of nervous cells is much faster (1 to 10 ms). It is believed that this signal results from changes in light scatter. In brain tissue, cellular membranes have refractive indices different from the refractive indices of the intra- and extracellular space, which leads to light scattering. It is therefore possible that changes in membrane potential associated with neuronal activity may lead to changes in the refractive properties of those membranes and therefore cause changes in light scattering. Another possible mechanism influencing light scattering

*Current Address: Department of Neurology and Brain Imaging Center, Goethe University, Frankfurt, Germany.

Address all correspondence to: Andrei V. Medvedev, CFMI, GUMC, Preclinical Science Building, LM 14, 3900 Reservoir Road, NW, Washington, DC 20057. Tel: 202-687-5126; Fax: 202-687-7906; E-mail: am236@georgetown.edu.

is related to changes in cell volume. Although discovered earlier than the hemodynamic optical signal,¹ the so-called fast optical signal (FOS) remains controversial when an attempt is made to record it noninvasively from the scalp.

During the last 10 years, there have been several attempts to record fast optical signal noninvasively through the scalp and skull in human subjects.^{12,15–23} The results of these studies, however, have been controversial. Using phase measurement with a frequency-domain optical instrument, Gratton et al.¹⁵ reported short-latency and well-localized event-related optical signal (EROS) recorded from the human occipital cortex during visual stimulation. This response showed spatial agreement with an fMRI signal and temporal agreement with a visual evoked potential. Since then, several reports replicating and expending the initial results have been published by the same group, including recording of the fast optical signal from the auditory cortex during auditory processing and motor cortex during somatosensory stimulation.^{16,20,24}

Steinbrink et al. were first to measure fast optical signals using a continuous-wave (CW) optical instrument and intensity measurements ($\Delta I/I$), rather than photon delay,¹⁷ but subsequent results reported by this group have been less consistent. A more recent study has yielded limited results, as the authors detected a significant change in optical signal in only one from eight subjects during subthreshold median nerve stimulation and a lack of signal in all 11 subjects during visual stimulation with reversing checkerboard.²³ Importantly, the authors emphasized the problem of motion artifacts in optical recordings and cautioned that even small stimulus-correlated movement artifacts may potentially mimic fast optical signals.

In a study by Franceschini and Boas,¹² fast optical signal was recorded in 10 healthy volunteers during finger-tapping, tactile stimulation, and electrical median nerve stimulation using a CW instrument. The fast signal was detected in 43% of the measurements during finger-tapping, 60% of those during tactile stimulation and 23% of those during electrical median nerve stimulation. The relative changes in intensity associated with brain activation were $\sim 0.07\%$ with latencies ~ 100 ms (Ref. 12). However, a recent study by the same group has failed to detect EROS in optical signals recorded in two monkeys epidurally—i.e., at the exposed surface of the brain dura mater during visual stimulation with a reversing checkerboard.²⁵

Morren et al.²² used a frequency-domain system and measured the amplitude, mean intensity, and phase of the optical signal during a finger-tapping task. The authors employed sophisticated data analysis algorithms—namely, an adaptive filter and independent component analysis (ICA) to remove arterial artifacts from the optical signals. In 9 of 14 subjects, a significant fast neuronal signal related to the finger tapping was found in the intensity signals. In the phase signals, indications of the fast signal were found in only two subjects.²²

Thus, because FOS has been demonstrated in several but not all studies where an attempt was made to record it, it is important to extend the scope of experimental paradigms in order to further explore the detectability of FOS and find optimal conditions as well as signal processing algorithms, which may be necessary for its reliable recording. Given a significant problem with motion artifacts potentially mimicking fast signals, in the current study, we have decided to use a Go-NoGo paradigm where a motor response is required in response to only one class

of stimuli (targets). Different from the most commonly used electrophysiological paradigm of an oddball task where target stimuli constitute only a small portion of all stimuli, in the Go-NoGo task, the numbers of targets and nontargets are often similar. This is optimal for the comparison between target- and nontarget-related brain responses when only targets require an overt motor response.

In the Go-NoGo paradigm, participants are asked to respond to one class of stimuli ("target" or "Go"), e.g., by pressing a button, and to withhold their response to another class ("nontarget" or "noGo").²⁶ Using event-related potential (ERP), it has been well established that noGo responses (in comparison with Go responses, i.e., when a noGo > Go difference is calculated) evoke a large negativity around 200 to 300 ms (depending on the task) over frontal sites with a corresponding positivity at occipital sites,²⁶ a response termed a "N200 noGo effect."²⁷ If the opposite contrast is used (Go > noGo), differential activity is observed at 200 to 300 ms as a negative potential over temporal-occipital and positive deflection over frontal regions.²⁸ Because its electrophysiological correlates are well known, this task provides a good opportunity for a search for the corresponding correlates within FOS. Thus, a more specific goal of the study was to find an optical analog (if any) of the N200 ERP component and test whether it has physiological properties similar to the N200 potential—namely, whether its amplitude is sensitive to the stimulus class (target versus nontarget) and whether its timing correlates with a behavioral response.

In the following text, we refer to the raw and preprocessed electrical and optical data as "EEG" and "FOS," respectively, and to the event-related data (i.e., after trial averaging) as "event-related potential" (ERP) and 'event-related optical signal' (EROS). When describing individual components/waves of EROS, we utilize a commonly used ERP naming convention and add the letter "o" at the front of the corresponding ERP name. For example, an optical analog of the N200 ERP component is referred to as "oN200."

2 Methods

Our experimental approach has been described in detail elsewhere,²⁹ and here we provide a brief description of the methods.

2.1 Participants and Recording Probes

Experiments were performed with participation of 11 right-handed individuals (five females; mean age 23) who signed the consent form approved by Georgetown University Institutional Review Board. All participants reported normal (or corrected to normal) vision and performed a battery of behavioral tests including the assessment of IQ and handedness. Before the experiment (lasting up to 2 h), an electrode sensor net was placed on the subject's head with 128 channels for EEG recording: [manufactured by Electrical Geodesic, Inc. (EGI), Eugene, Oregon]. On top of the EEG net, two optical probes were placed that were specifically designed for simultaneous acquisition of optical and EEG signals. Lightweight flexible optical fiber bundles (~ 2 mm in diameter) had their front ends (optodes) bent at a right angle at the length of 18 mm to allow them to reach the scalp through the EEG net. Optodes were arranged on a supporting

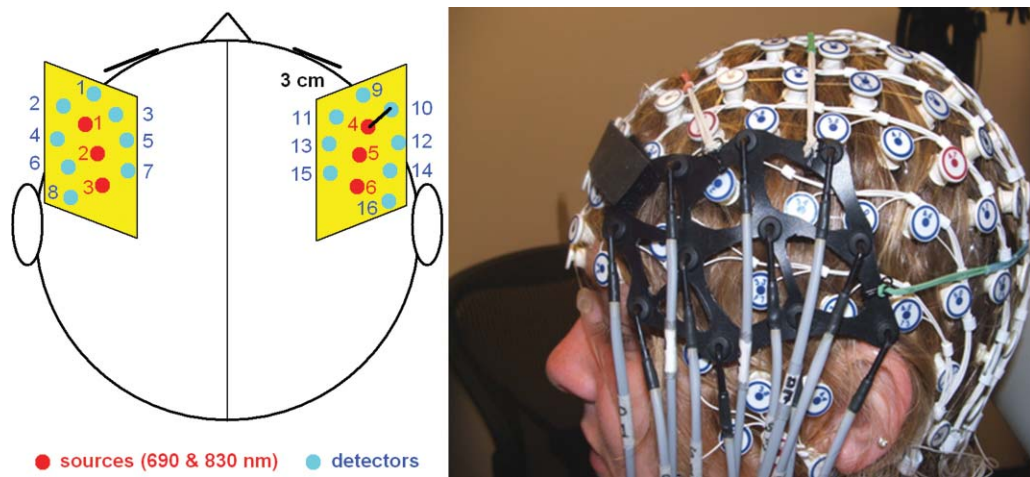


Fig. 1 (a) Positions of laser sources (red/black) and detectors (blue/gray) on the scalp. (b) Optical probe on top of the EEG sensor net. (Color online only.)

flexible plastic base (15×8 cm) holding three source fibers and eight detector fibers (Fig. 1). Two such probes were placed bilaterally on each side of the head to cover the inferior and the middle frontal gyri (IFG and MFG, respectively) using the EGI electrodes as reference points in relation to the anatomical landmarks of the international 10–20 EEG system. The area covered by the left probe extended from the Fp1 to T3 location along the anterior–posterior axis and from the F7 to F3 location along the ventral–dorsal axis. The right probe was placed symmetrically.

2.2 Experimental Paradigms

The Go-NoGo task was based on a paradigm introduced by Thorpe et al.²⁸ to study rapid detection of familiar objects (animals). Black-and-white pictures of natural scenes (size 472×728 pixels) normalized by brightness and contrast were presented on a computer LCD monitor at a viewing distance of 75 cm and an angular size of 10 deg. To minimize expectancy effects, stimulus onset asynchrony (SOA) was varied randomly from 900 to 1700 ms. Stimulus presentation was organized in 12 blocks, each containing 100 pictures. There were short periods of rest (~ 10 s) after each block and longer rest periods (30 to 60 s) between series of four blocks. Subjects were instructed to detect whether an animal (target) was present in the picture displayed for 26 ms and, in response to targets only, press two buttons on a button box using both thumbs as soon as possible. Between picture presentations, a crosshair was displayed in the center of the monitor, and subjects were instructed to fix their gaze on the cross to minimize eye movements.

2.3 Data Collection and Analysis

Optical signals were recorded with a continuous-wave CW5 imaging system (TechEn, Inc., Milford, Massachusetts). The system has 32 laser sources emitting light at two wavelengths, 690 nm and 830 nm (i.e., 16 lasers at each wavelength), and 32 avalanche photodiodes as detectors. Data collection from all detectors is performed in parallel at a high sampling rate (41.7 kHz). Each laser is modulated at a different frequency from 6.4 kHz to 12.8 kHz, with intervals of 200 Hz between adjacent channels to allow subsequent offline frequency de-

modulation and separation of individual source–detector pairs. In current experiments, only three dual-wavelength (690 and 830 nm) laser sources and eight optical detectors for each hemisphere were used. Synchronization of picture presentation and data acquisition was achieved using a standard transistor-transistor logic (TTL) trigger pulse generated by the presentation software (E-Prime) at the onset of picture presentation. At this time, a square sound wave (20-ms duration) was also sent by E-Prime to the analog output of the computer sound card. The trigger pulse was recorded by the EEG instrument, and the square sound wave was recorded at the auxiliary channel of the CW5 instrument for event-related synchronization of optical data using the rising edge of the sound wave.

After frequency demodulation and disentanglement of source–detector pairs, 28 channels for each wavelength were selected for further analysis (four nearest detectors d1 to d4 for source s1, six nearest detectors d3 to d8 for source s2, and four nearest detectors d5 to d8 for source s3 give 14 channels plus 14 homologous channels from the right hemisphere; see Fig. 1). Optical data were then separated into slow (hemodynamic) and fast components. Because optical amplitude measurements provided by CW instruments do not allow the experimenter to distinguish between light absorption (the major source of a hemodynamic signal) and light scatter (a presumed source of fast optical signals), we used a simple empirical approach based on signal filtering. To get the slow component, the optical signal was lowpass filtered at <1 Hz. To get the fast component, the same raw signal was filtered within 2 to 100 Hz. The cutoff frequency of 2 Hz was chosen in order to reduce cardiac artifacts significantly present within optical signals. Further elimination of cardiac artifacts was done through independent component analysis (ICA).³⁰ We used the FastICA algorithm available as a package of MATLAB scripts at <http://www.cis.hut.fi/projects/ica/fastica>. The slow (hemodynamic) signal was downsampled at 20 Hz, analyzed separately, and presented elsewhere.²⁹ Here, we present only the fast signal along with the EEG data. The fast optical signal was downsampled at the same sampling rate used for EEG data acquisition (200 Hz). EEG data was bandpass filtered at 1 to 100 Hz. Both FOS and EEG signals were segmented into

stimulus-related trials using a time window (-200 – 800 ms around the onset of picture presentation (assumed to be at $t = 0$). All trials were joined together in a correct sequential order to produce “preprocessed” or segmented data. Independent component analysis was then performed on the segmented data (separately for EEG and for each wavelength of FOS). Artifactual ICA components were identified as related to cardiac activity (the most pronounced artifact in FOS), eye blinks and eye movements (the most pronounced artifacts in EEG), and small sporadic head movements (present in both FOS and EEG). All these artifacts were removed during restoration of FOS and EEG signals from their corresponding ICA components. Before averaging over trials, FOS and EEG data were converted to “baseline-based” z-scores at each trial. First, baseline correction was done. [The mean value over a baseline period (-200 – 0 s was subtracted from the signal amplitude at each time point.] Then, the signal was normalized by dividing its amplitude at each time point by the standard deviation calculated over the baseline period. Z-score normalization allowed us to directly compare optical and electrical signals as well as served as an estimate of the signal-to-noise ratio (SNR), because standard deviation of the signal over baseline periods is a direct measure of noise. Also, such normalization made all channels comparable to each other regardless of their “optical impedance” (a reversal of tissue transparency), which renders signals at different detectors to have different amplitudes (sometimes by several orders of magnitude), depending on the thickness of the overlaying layers (scalp and skull).

Last, event-related averaging for target trials and nontarget trials was performed taking into account only correct trials—namely, target trials when the subject did produce a motor response (indicating correct detection of a target) and nontarget trials when the subject withheld his/her response. Incorrect trials with both false-positive and false-negative errors were excluded from the analysis. Statistical analysis was performed within each subject first, and then individual EROS and ERP waveforms were averaged over all subjects, resulting in grand average waveforms. Group analysis was done using a nonparametric Mann-Whitney test with either 1% or 5% significance level. The test was applied for each time bin within a trial epoch, as suggested by Thorpe et al. for ERP analysis.²⁸ Namely, EROS was considered “detected” in a particular subject if its amplitude was significantly different from zero in at least five consecutive time bins within the time window of 100 to 500 ms in at least one channel within the group of anterior channels (channels s1-d1:d4 in the left hemisphere and channels s4-d9:d12 in the right hemisphere where some degree of activation was observed in all subjects). This way, we also reduced the number of multiple comparisons, making our statistical criteria more robust. Last, 3-D scalp maps for visualization of spatial distribution and temporal evolution of task-related prefrontal activity were produced using interpolation and projection of grand average EROS onto a normalized head template available in the open-source EEGLAB software.³¹

3 Results

All participants successfully performed the task, producing a relatively small number of errors ($\sim 1.8\%$). The average reaction time (RT) was 419 ± 44 ms (mean \pm standard deviation).

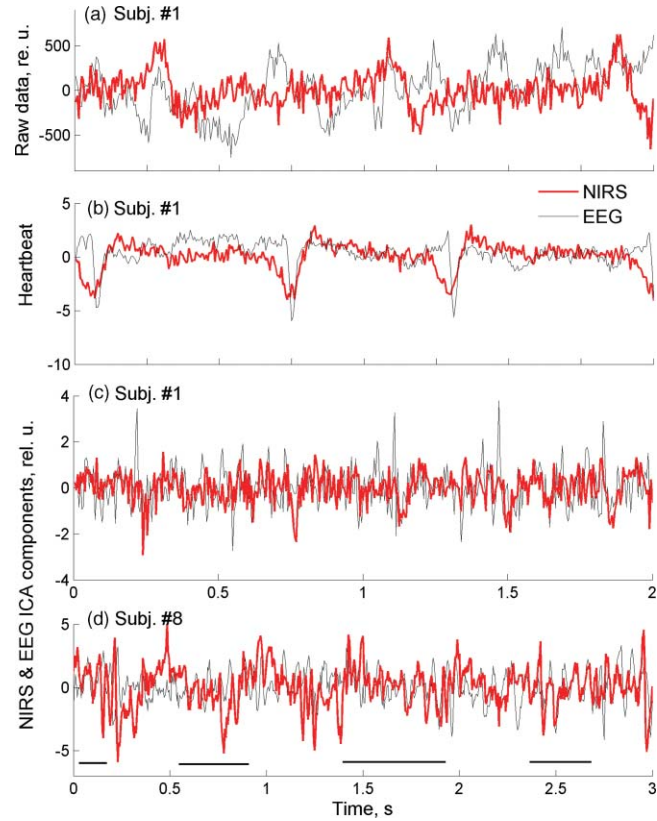


Fig. 2 Representative segments of EEG (gray/thin line) and FOS (red/thick line). (a) Raw data. (b) Independent components of EEG and FOS containing the cardiac artifact. (c) and (d) The best correlated EEG–FOS pairs from two subjects. Horizontal lines in (d) indicate segments with a good match between individual waves of FOS and EEG. (Color online only.)

3.1 Analysis of Independent Components of FOS and EEG

Representative segments of preprocessed optical and electrical signals shown in Figs. 2(a) and 2(b) illustrate that the raw FOS and EEG data were not correlated except for common artifacts present in both modalities [e.g., cardiac artifacts; Fig. 2(b)]. When applying the ICA algorithm, the number of independent components (ICs) should be set as a parameter. Because this number is not known *a priori*, it is usually taken equal to the number of data channels. Therefore, EEG data were decomposed into 127 independent components (128 channels of EEG data re-referenced to the common average give 127 independent channels), and FOS data were decomposed into 28 ICs for each wavelength. ICA components containing mostly artifacts were identified through visual inspection and spectral analysis and removed during signal restoration, as described previously.³² For EEG, 40 to 80 ICs, and for FOS, 3 to 6 ICs for each wavelength were removed as artifactual in each subject. An example of ICs for EEG and FOS, both containing the same cardiac artifact, is shown in Fig. 2(b). To estimate the effect of artifact removal, which was most critical for the detectability of FOS, we used weights within the ICA weight matrix (described in our previous study³²) “belonging” to the removed artifactual components and showing their relative contribution to the raw signals. A sum of those relative weights indicates a relative contribution of removed artifact and noise components into the total variation of

Table 1 Noise reduction (%) in the FOS as a result of ICA-based artifact removal and normalized ERP and EROS amplitudes (relative units) calculated for all subjects. The greatest and the smallest amplitudes for each modality (electrical and optical) are shown in bold.

Subject No.	1	6	7	8	14	23	24	25	26	27	28	Mean	St. D.
FOS noise reduction	66	86	66	73	76	65	79	70	64	73	65	71	7
ERP	1.4	0.84	1.22	0.88	1.06	1.22	1.35	1.95	1.76	0.79	0.83	1.21	0.39
EROS	0.62	0.3	0.76	0.5	0.4	1.02	0.28	0.23	0.97	0.53	1.8	0.67	0.46

the signal and was used as an estimate of noise reduction in each subject. On average, noise reduction was $71 \pm 7\%$ (Table 1), which translates into a factor of $1/0.29$ in signal-to-noise ratio—i.e., a 3.4-fold increase.

After artifact removal, all optical and EEG independent components were correlated pairwise over all 1200 trials, and the best correlated EEG–FOS pair was identified for each subject. The correlation coefficient for the best correlated EEG–FOS pairs reached ~ 0.1 and was highly significant in every subject. To take into account multiple pairwise correlations between artifact-free EEG and FOS ICs (approximately $80 \times 25 = 2000$ correlation coefficients in each subject), we used the Bonferroni criterion for group-wise corrections, and even after correction, a significance level for the best correlated pairs was very high ($p < 10^{-8}$). For additional control for group-wise errors, we also did simulations of white-noise signals with the same sampling rate (200 Hz) and of the same duration (1200 one-second trials) and calculated pairwise correlations between those noise signals. Correlation coefficient for noise signals varied from -0.02 to 0.02 , and the Bonferroni-corrected p -value was insignificant ($p > 0.05$). Although not high in absolute terms (~ 0.1),

highly significant correlation of optical and electrical signals was a result of a good “match” between the best correlated components of FOS and EEG, which could be visually observed over all 1200 trials, often showing a “wave-to-wave” correspondence between individual EEG and FOS waves [Figs. 2(c) and 2(d)].

Independent components of EEG and FOS were averaged separately over target and nontarget trials in each subject and analyzed for a stimulus-related response. Using the “5-bin” criterion described earlier, statistically significant event-related responses were found in all subjects. Typically, only some independent components (from the total number of ~ 25 for each wavelength of FOS and of 40 to 80 ICs for EEG) showed significant responses to the stimulus, as demonstrated by examples from two subjects shown in Fig. 3. For direct comparison between EEG and FOS components, we selected the optical component showing the best response and found an EEG component best correlated with it using the correlation matrices shown as insets in Fig. 3. The temporal profiles of optical ICs with responses appeared to be very similar to the profiles of the corresponding electrical ICs (Fig. 3, bottom). It is important to

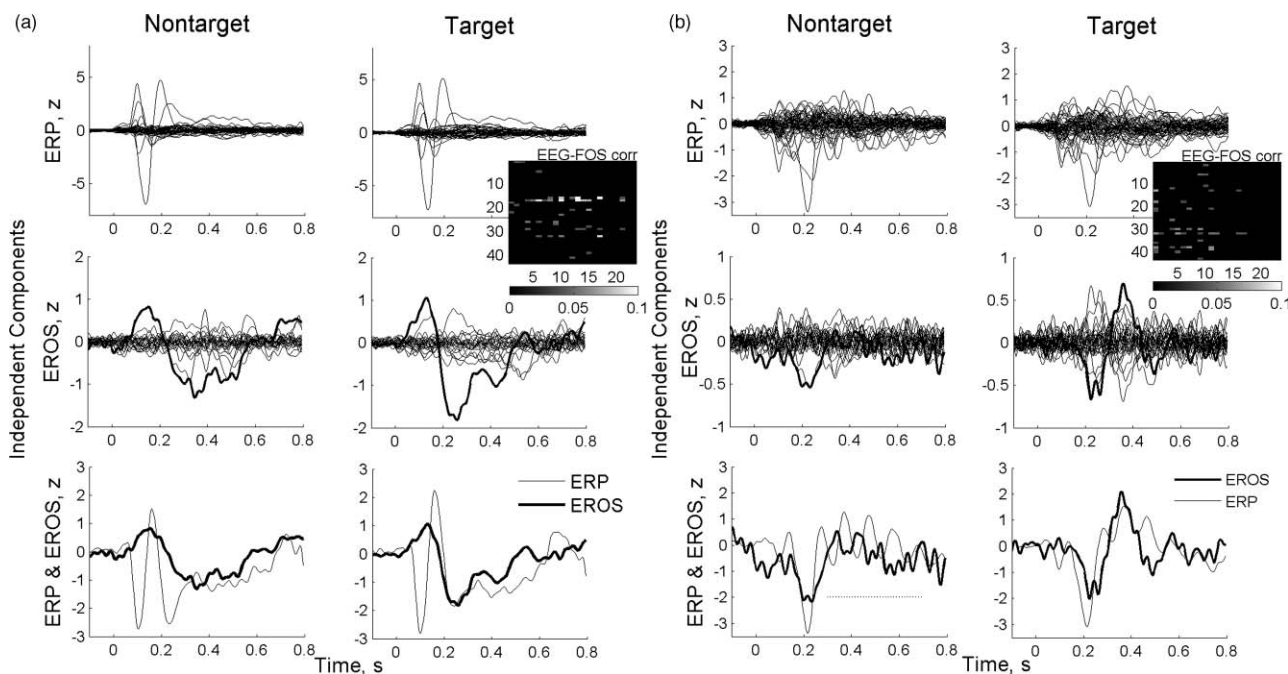


Fig. 3 Representative examples of event-related responses (produced by trial averaging of independent components of EEG and FOS) from subjects 28 (a) and 1 (b). Best optical responses are shown in bold. Note a good correspondence between the temporal profiles of the best correlated ERP and EROS components (bottom panels) as well as similar responses for targets and nontargets. Insets show matrices of correlation coefficients between all remaining EEG (the ordinate) and FOS (the abscissa) independent components. Matrices show only correlation coefficients with absolute values significantly different from zero ($p < 0.001$ after Bonferroni correction).

note that optical components did not necessarily follow the corresponding ERP waveforms exactly but matched more closely an ERP envelope, as illustrated in Fig. 3(a). Also, individual FOS waves might be either in phase or out of phase with the corresponding EEG waves, as illustrated in Fig. 3(b), bottom. In this example, the N200 wave is negative for both ERP and EROS, while an immediately following burst of alpha activity (~ 10 Hz) within the ERP is out of phase with the corresponding burst of similar "alpha-like" activity within the EROS. (This burst of alpha activity is marked by a dotted line in Fig. 3, bottom left.)

3.2 EROS and ERP in Individual Subjects

After artifact removal, FOS and EEG signals were restored from the remaining independent components and obtained artifact-free signals were averaged over all trials and subjects, giving individual and grand average ERP and EROS waveforms for each recording channel. As a result, we were able to analyze spatial distribution of EROS over all recording sites. Importantly, EROS was observed in just one or a few channels. Highly compact localization of EROS is illustrated in Fig. 4, which shows four anterior optical channels formed by one source (s1 or s4) and four surrounding detectors (d1–d4 and d9–d12) in the left and right hemisphere, respectively, in one subject. A clear response was observed in channel s4-d10 only, being almost absent in all neighboring channels as well as in the contralateral hemisphere.

Figure 5 shows EROS waveforms from four representative subjects. Of those, subject 28 had the largest EROS amplitude [the "best" subject; Fig. 5(c)] and subject 25 had the lowest EROS amplitude [the "worst" subject; Fig. 5(d)]. (Maximal EROS amplitudes for all subjects are presented in Table 1.) These examples demonstrate both similarity and interindividual variability of optical responses. First, we note almost identical EROS waveforms at both wavelengths, which slightly differed in signal amplitude only (Fig. 5). Second, several typical components of EROS were identified within those individual (i.e., subject-specific) responses, which were similar to

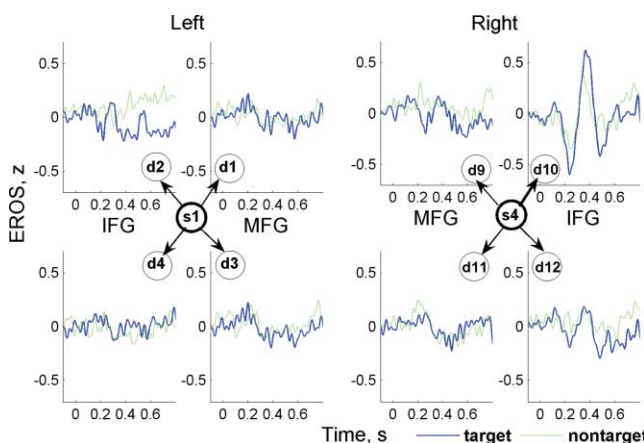


Fig. 4 EROS was well localized, as illustrated by its presence in only one channel in this subject. Here, from four detectors (d9–d12) surrounding one source (s4) in the right hemisphere, EROS was observed in channel s4-d10 only, being almost absent in all neighboring channels. IFG and MFG are the inferior and the middle frontal gyri, respectively.

the corresponding ERP components. (Here and in the following, by the term "component" we refer to distinct waves within an ERP or EROS waveform, which is different from "independent components" resulting from independent component analysis; describing ERP and EROS waveforms, we will use the terms "components" or "waves" interchangeably.) Thus, after an initial transient increase in optical signal at $t = 100$ ms (optical positive wave termed "oP100"), the most robust and stable optical component was observed at $t = 200$ to 300 ms as a negative wave due to a decrease in signal amplitude (oN200). The oN200 wave was followed by oP400, oN500, and oP600 waves (Fig. 5). All EROS components varied by amplitude between subjects. For example, the earliest component oP100 was large in subject 28 [Fig. 5(c)], being weaker in subject 1 [Fig. 5(a)], and almost absent in subjects 8 and 25 [Figs. 5(b), 5(d)]. Similar variability was observed for later components. For example, the oP400 and oN500 waves were large in subjects 1 and 8, while being hardly observable in subject 28. The oN200 component was most stable and observed in all subjects including subject 25, who had the lowest EROS amplitude [Fig. 5(d)]. Third, EROS was well localized (observed in one or a few anterior channels) in all subjects.

To further test reliability of optical signals, we also calculated EROS using smaller subsets of trials ($n = 100$) randomly selected from all trials in each subject. For comparison reasons, the corresponding EROS waveforms calculated over 100 trials from the same subjects as in Fig. 5 are shown in Fig. 6 (for wavelength 830 nm, which typically showed larger responses). It can be seen that EROS was reliably recorded over only 100 trials with a significant deviation from zero at the 5% significance level in all subjects (Fig. 6). Also, the graphs in Fig. 6 are plotted with the same amplitude scale to demonstrate how much normalized EROS amplitude varied between subjects. The maximal EROS amplitude for each subject was calculated by taking

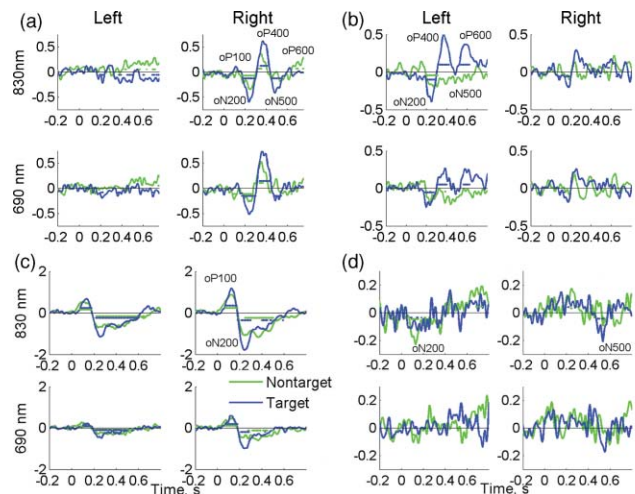


Fig. 5 EROS waveforms recorded from subjects 1 (a), 8 (b), 28 (c) and 25 (d). Each panel shows signals at two wavelengths from the best channel and its counterpart in the opposite hemisphere. Note the almost identical waveforms and similar responses for targets (blue) and nontargets (green). Horizontal lines in each graph indicate the time bins where EROS was significantly different from zero [(a) to (c): $p < 0.01$ for subjects 1, 8, and 28, and (d): $p < 0.05$ for subject 25 with the lowest SNR]. (Color online only.)

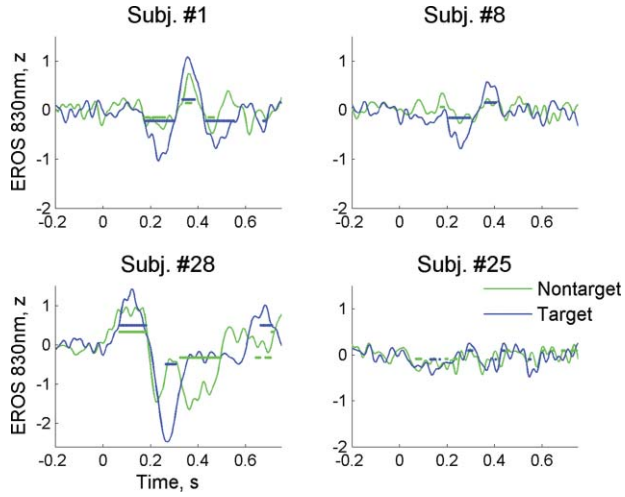


Fig. 6 EROS waveforms recorded from the same subjects presented in Fig. 5 using 100 trials for each stimulus class (target and nontarget) randomly selected from all available trials. Horizontal lines in each graph indicate the time bins where EROS was significantly different from zero ($p < 0.05$).

the maximum of the absolute value of EROS over time period 100 to 600 ms. These values were compared with the signal amplitudes calculated similarly for ERPs (Table 1). Compared to the highest amplitude in subject 28 [Fig. 5(c) and Fig. 6(c)], the lowest amplitude in subject 25 [Fig. 5(d) and Fig. 6(d)] was $\sim 85\%$ lower. On average, the normalized EROS amplitude was comparable to the normalized ERP amplitude (0.67 for EROS versus 1.21 for ERP; Table 1). Interindividual signal variability was greater for EROS compared to the ERP (standard deviation of 0.46 for EROS versus 0.39 for ERP; Table 1).

3.3 Grand Average EROS and ERP and Their Correlation with a Behavior Response

Grand average EROS and ERP waveforms (i.e., averaged over all subjects) showed good temporal correspondence between the individual components present in both signals (Fig. 7). Moreover, differential responses (targets versus nontargets) were similar in both modalities. The earliest differences between target- and nontarget-related responses were observed during oN200/N200 waves (significant in the left hemisphere for EROS, Fig. 7(a), and in both hemispheres for ERP, Fig. 7(b)). The peaks within differential responses ("target ERP minus nontarget ERP" and "target EROS minus nontarget EROS") occurred at the same time (indicated by arrows in Fig. 7). Behavioral response (at $t = 419 \pm 45$ ms) was followed by the late waves developed over time interval 500 to 600 ms. Those late waves also showed significant differences between targets and nontargets (in the right hemisphere for EROS and bilaterally for EEG; see Fig. 7).

Given the sensitivity of oN200/N200 components to the stimulus class, we predicted a relationship between the timing of both signals and the reaction time of a behavioral response. The rationale is that if the N200 wave is a marker of an object recognition event, then a decision about a response is made at about the same time. We therefore tested whether there was a relationship between the differential (target > nontarget) oN200/N200 waves

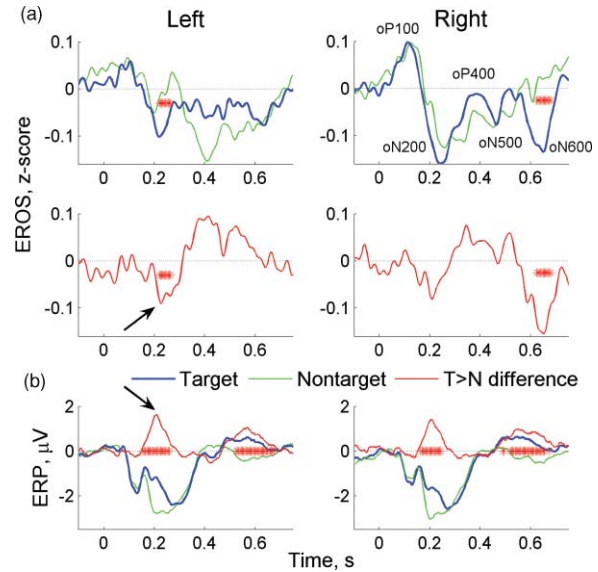


Fig. 7 Grand average EROS and ERP. Asterisks show time bins where the difference between targets and nontargets was significant ($p < 0.05$). Arrows point to the early peaks in differential responses.

and the reaction time measured for each subject. In addition, we tested whether the times and amplitudes of oN200 and N200 waves correlated with each other. Thus, several correlations were analyzed—namely, (1) a relationship between subject's reaction time and the oN200 peak time [Fig. 8(a)]; (2) a relationship between subject's reaction time and the N200 peak time [Fig. 8(b)]; (3) a relationship between the peak times of oN200 and N200 waves [Fig. 8(c)]; and (4) a relationship between the amplitudes of differential oN200 and N200 waves (Fig. 9(d)]. Significance of correlations was assessed using ANOVA test for the slopes of regression lines being significantly different from

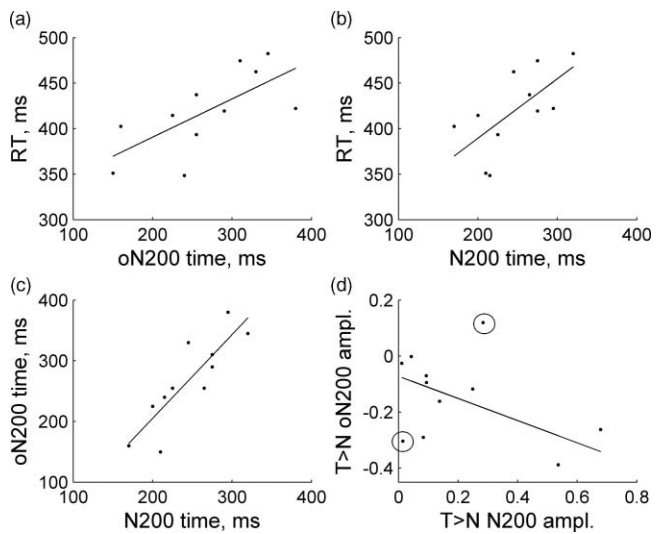


Fig. 8 Group-level regression analysis on correlations between the timing of target-related oN200/N200 waves and the reaction time [(a) and (b)] and between the timing/amplitudes of oN200 and N200 waves with respect to each other [(c) and (d)]. Circled points in (d) are outliers that were discarded during statistical analysis of this particular regression.

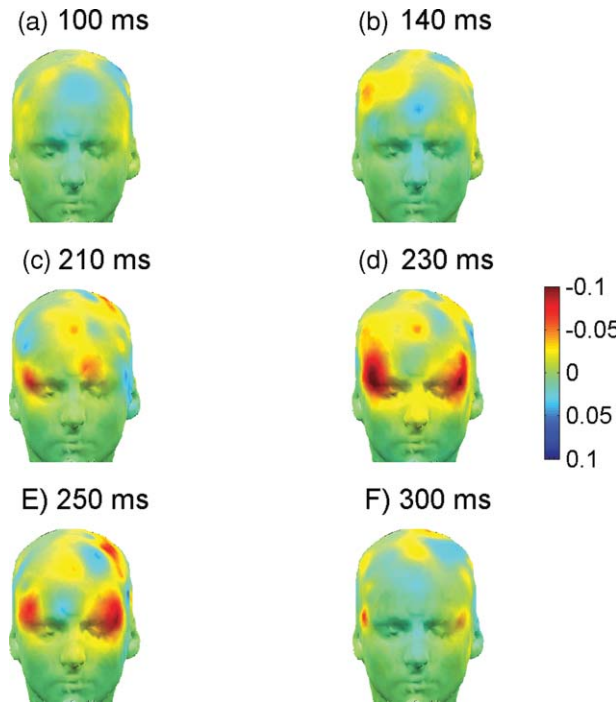


Fig. 9 Temporal evolution of frontal activation during target detection in the Go-NoGo task through optical imaging with the fast signal. Scalp maps of grand average differential EROS (targets versus nontargets) are produced by interpolation and projection of signal amplitude onto a human scalp template. Note initial activation in the right prefrontal cortex at 140 to 210 ms followed by coactivation of the homologous area in the left hemisphere at 230 to 250 ms.

zero. The first three relationships were significant: (1) $F = 8.0$, $p = 0.02$; (2) $F = 7.1$, $p = 0.026$; and (3) $F = 25.0$, $p = 0.0007$. For the third relationship (between the oN200 and N200 peak times), the regression line slope was not significantly different from 1 (the lower and upper 95% limits were 0.75 and 2.0, respectively), and the regression line intercept was not significantly different from 0 (the lower and upper 85% limits were -226 ms and 84 ms). Thus, the peak times of oN200 and N200 waves were statistically close to each other. There was also a tendency for a correlation between the amplitudes of differential oN200 and N200 waves, but this correlation did not reach significance because of a relatively large interindividual variation in the signal amplitudes. However, with two outliers removed [the circled points in Fig. 8(d)], this regression line is significant ($F = 7.2$, $p = 0.03$).

Differential (target > nontarget) scalp maps of EROS showed no difference between target- and nontarget-related responses up to 100 ms [Fig. 9(a)], with a first sign of divergence in the right middle frontal cortex at about 140 ms after the stimulus [Fig. 9(b)]. Then the focus of activation moved into the right inferior frontal cortex at 210 ms [Fig. 9(c)]. At its peak and after (230 to 250 ms), activation spread to the left inferior cortex and thus became bilateral [Figs. 9(d) and 9(e)] gradually wearing off within 250 to 300 ms [Fig. 9(f)].

4 Discussion

In the current study, we recorded fast optical signals from prefrontal cortex in combination with high-density EEG during a

Go-NoGo task. Simultaneous recording of brain activity in two different modalities (optical and electrical) allowed us to directly compare and verify FOS with EEG. For the first time, a significant correlation was demonstrated between electrical and optical signals recorded noninvasively from the scalp. Using independent component analysis, we were able to effectively remove artifacts from both EEG and FOS and reduce a total noise in the FOS by 71% (which translates into a 3.4-fold increase in SNR). As a result, EROS was reliably recorded in all subjects. Importantly, a significant correlation was found between independent components of optical and electrical signals. Moreover, this correlation was observed not only for event-related signals averaged over several hundred trials, but also for the preprocessed data before trial averaging (Fig. 2). Single trials stacked together showed a highly significant correlation between EEG- and FOS-independent components ($p < 10^{-8}$). Such high level of significance, despite a relatively low absolute value of correlation (~ 0.1), was due to the fact that "resemblance" between EEG and FOS was observed over all 1200 trials (240,000 data points). EEG signal is commonly viewed to be a result of spatiotemporal summation of postsynaptic membrane potentials mostly on large pyramidal cortical cells, and grossly reflects interaction of excitatory and inhibitory postsynaptic processes (see, for example, Ref. 33). We therefore conclude that at least some components of FOS recorded through the skull "reflect" electrical processes on neuronal membranes within the cortex. Therefore, FOS resembles an electroencephalogram (as in Fig. 2) and can be considered as an "optoencephalogram."

Trial averaging of independent components of FOS and EEG revealed a relatively small number of those components that showed a response to the stimulus. Temporal profiles of those "event-related components" were similar for EEG and FOS (Fig. 3). Such a similarity between evoked electrical and optical signals is demonstrated for the first time and can be compared to the close match between neuronal action potentials and their optical analogs demonstrated in neuronal cultures by Stepnoski et al.³⁴ It should be noted, however, that optical signals did not necessarily match ERP waveforms exactly but sometimes resembled ERP envelopes, as in Fig. 3(a). It is well known that a dipole nature of the ERP leads to a complex distribution of electric fields over the depth of the cortex and, as a result, to a complex relationship between the polarity of ERP components recorded at the scalp and the intracortical positions of their generators. It is unknown whether an optical signal recorded through the skull is able to fully reflect this complex relationship. Therefore, one cannot expect to see a close match between EEG and FOS. For example, it is likely that optical signal can be either in-phase or out-of-phase with ERP waves. This may lead to a more "loose" relationship between EEG and FOS waveforms and can explain a relatively low correlation between EEG and FOS observed in the current study (~ 0.1). Nonetheless, a significant correlation between EEG and FOS is remarkable, and quite often a good match between individual optical and electrical waves can be seen [Figs. 2(c) and 2(d)]. Another example is in the bottom-left panel of Fig. 3(b). Here, a stimulus-related response (negative wave around 200 ms) was followed by a burst of alpha activity (4 to 5 oscillations at frequency ~ 10 Hz well seen in the ERP and marked by a horizontal dotted line). A similar burst of "alpha-like" waves was also seen within EROS being out-of-phase with the ERP burst [Fig. 3(b), bottom left].

In many previous studies of fast optical signals, the investigators have used simpler ("less cognitive") tasks [e.g., sensorimotor stimulation, sensory (visual or auditory) stimulation, or oddball tasks] and recorded from sensorimotor and/or primary visual cortex.^{12,15-23} We are aware of only one study where fast optical signal was recorded in the dorsal frontal cortex during an auditory oddball task.³⁵ Frontal cortex is engaged in a large variety of cognitive tasks, and it is important to demonstrate reliable fast signals in this area. During oddball tasks when targets are rare (10 to 20% of all stimuli), only responses to targets have been reported (see, for example, Ref. 35 and also our previous study, Ref. 32). In the current study, responses were observed for both targets and nontargets, which was likely to be due to an equal presence of targets and nontargets in the stimulus set (~50% each). Similarity of target and nontarget responses during Go-NoGo tasks is well established in electrophysiological studies.^{26,28} The Go-NoGo paradigm with two types of stimuli allowed us to compare target- and nontarget-related trials. Because nontarget stimuli were not accompanied by motor responses, nontarget-related trials served as a control without any possible contamination by motor artifacts. Given almost identical EROS waveforms for targets and nontargets (Figs. 3 and 4), which also corresponded well to the similarity of target- and nontarget-related ERPs, we are confident that optical responses observed in the current study were not produced by motor artifacts (for both targets and nontargets).

The current study demonstrated a highly compact localization of EROS. In the majority of subjects, a significant response was observed in just one channel of either the right or left hemisphere, in the homologous channels of both hemispheres or in two adjacent channels of one hemisphere. These observations confirm the previous findings with respect to high localization of EROS.^{15,20} For example, in the study by Gratton and Fabiani,²⁰ it has been demonstrated that EROS amplitude was reduced by 85% at 15 mm from the predicted peak location, suggesting that the spatial resolution of EROS is at least 1 to 2 cm (see also Ref. 35). In accordance with a well-known "banana-shaped" probabilistic map of photon penetration between the source and the detector demonstrated in Monte Carlo simulations (see, for example, Refs. 12 and 36), we assume that an optical "recording site" is positioned at the midpoint between the source and the detector (typically separated by 3 cm for scalp recordings). Taking into account a ~3-cm separation between neighboring detectors in our probes, we estimate that the area of reliable detection of EROS in the current study was well within 1.5 cm. This estimate is in excellent agreement with the estimate made by Gratton and Fabiani.²⁰ Such highly compact localization of EROS is intriguing and may be crucially important for its successful recording. We suggest that to a significant extent, the difficulty with reliable recording of EROS may be related to the localized nature of this signal. For example, Radhakrishnan et al. in a recent study²⁵ did not demonstrate EROS using optodes positioned on the dura mater of a monkey's brain through the "recording well" cemented on the skull above the primary visual cortex. The diameter of the optical probe was 1.7 cm, and two or three detectors were separated from a single source by 0.7 to 1.5 cm. Thus, the area of "optical coverage" was 1.5 cm in diameter. If the probe was not placed *exactly* above the predicted focus of cortical activation (which might be less than 1.5 cm in diameter), this may explain a negative result of

the study. [Another reason for the negative result may be related to insufficient tightness of the contact between optodes and the dura mater. Optodes were fixed to the recording well, which was cemented on the monkey's scalp. Therefore, possible small movements of the dura mater (for example, due to cardiac-induced brain pulsations), might have led to the leakage of light into the extracerebral space. This might be causing an (at least partial) optical short-circuit between the source and the detectors and thus rendering weak fast optical signals unrecordable, even in the face of reliable recording of hemodynamic responses.]

In the current study, signal at each trial was normalized by the signal standard deviation over a baseline period. Therefore, normalized amplitude provides an estimate of the SNR *in single trials*. This allowed for direct comparison between electrical and optical signals. Normalized EROS amplitudes after ICA-based removal of artifacts were comparable to the ERP amplitudes (0.67 versus 1.2; Table 1). This result illustrates a well-known fact that even electrical brain responses have a relatively low SNR (~1), and this is why calculation of ERPs requires averaging over many event-related trials ($n \sim 100$). Averaging reduces noise by a factor of $1/\sqrt{n}$, while the response remains approximately the same because of its time-locking to the stimulus. For example, in the current study, averaging over ~500 trials led to highly significant responses ($p < 0.01$ and, in some subjects, $p < 0.001$), thus increasing the SNR of the *averaged* response to 5 to 8 (as estimated by the corresponding *t*-scores). Similar values for "single trial SNR" for EROS and ERP is a somewhat unexpected finding given a commonly held view that fast optical signals recorded noninvasively have very low SNR. It should be noted, however, that a direct comparison between EEG and FOS has not been done previously, and the frame of reference has been usually based on a comparison of FOS with hemodynamic NIRS signals, which have higher SNR. Moreover, in four subjects (7, 23, 26, and 28), the EROS amplitude was within or very close to the ERP amplitude range (0.79 to 1.95; Table 1). The EROS amplitude range (0.23 to 1.8) was larger than the ERP amplitude range. Greater interindividual variability and smaller EROS amplitudes in some individuals observed in the current study were likely to be due to a highly compact localization of EROS and inaccuracy in probe positioning with respect to the EROS peak location. We estimate the accuracy of our probe positioning as being about 1 cm. This might well have affected the recorded EROS amplitude. Indeed, in some subjects, we observed approximately equal EROS amplitudes in neighboring channels (for example, in channels s4-d9 and s4-d10; see Figs. 1 and 4 for channel positions). It is likely that the EROS peak location was between channels in those individuals, and this caused a decrease in EROS amplitude. Despite somewhat lower EROS amplitudes compared to the ERP, a statistically significant fast signal was recorded in all subjects even using only 100 trials (Fig. 6), which is a number of trials commonly used in the ERP studies. This result again demonstrates a relative reliability of fast optical signals, provided that adequate tools for artifact removal such as ICA³² or adaptive filtering^{37,38} are used.

EROS waveforms in all subjects were almost identical for wavelengths both shorter (690 nm) and longer (830 nm) than the isosbestic point of hemoglobin. The same-sign effect for two wavelengths points to light scattering as a more likely

mechanism for the observed fast signal rather than rapid de-oxygenated effects.³⁹ Indeed, hemodynamic processes accompanied by changes in blood oxygenation lead to changes in light intensity that are opposite (e.g., decrease and increase) at wavelengths on the opposite sides of the hemoglobin isosbestic point. Light scattering, on the other hand, leads to the same-sign effects observed at both wavelengths. The current study, therefore, provides further support for light scattering as an underlying mechanism for fast signals.

In the previous studies, which used either CW instruments (allowing only intensity measurements) or AC measurements with frequency-domain instruments (usually in addition to phase measurements), fast optical signal was observed as an event-related transient *decrease* in light intensity.^{12,17,32,35,39} A new observation made in this study is that EROS may have components/waves of both signs—i.e., negative and positive—which correspond to decreases and increases in light intensity, respectively. Although the most robust and stable EROS wave observed in this study was *negative* (oN200), we believe that positive components may also represent an important part of the optical signal. Indeed, both negative and positive optical waves correlated with the corresponding ERP waves (Fig. 3). Although a relationship between EROS and ERP may be extremely complex and indirect, there is at least a theoretical possibility for the fast optical signal to have not only a negative but also a positive sign. Indeed, Monte Carlo simulations demonstrate that the “banana-shaped” area representing a spatial profile of photon migration due to scattering effects has both negative and positive regions.¹² Thus, it is likely that both positive and negative deviations in EROS may be observable depending on the exact location of activated cortical areas in reference to the location of the source-detector pair.

Comparing EROS to ERP, we were able to identify several components/waves within EROS that were closely matching the corresponding ERP components. Referring to individual waves within EROS, we follow the naming convention used in the ERP studies. The earliest wave (oP100) was observed at about 100 ms after the stimulus and was followed by later components oN200, oP400, oN500, and oP600. Interindividual variations in EROS were also comparable to those seen in the ERPs. The most robust and stable component (oN200) was observed in all subjects, and it showed a sensitivity to the cognitive aspect of the task. The oN200 wave was larger for targets, and a differential (target > nontarget) oN200 wave peaked at $t = 225$ ms. Similarly, a peak in the target > nontarget difference was observed in the N200 component of the ERP. After a behavioral response, another time period with a significant difference between targets and nontargets was observed in the ERP at $t = 500$ to 700 ms. This differential response also had an optical analog observed at $t = 600$ to 700 ms in the right hemisphere [Fig. 7(b)]. The finding that the early difference between targets and nontargets was greater and significant in the left hemisphere points to the important role of the left hemisphere in object recognition, which is discussed in more detail in the following.

Regression analysis on a group level (over all subjects) demonstrated several important relationships between brain signals and behavior as well as between EROS and ERP. The finding that the reaction time correlated with the peak times of oN200/N200 waves confirms an important role of the N200

wave as a neurophysiological marker of brain processes involved in rapid object recognition. The peak time of the oN200 wave was highly correlated with the peak time of the N200 wave [Fig. 8(c)]. In addition, the amplitudes of differential (target > nontarget) oN200 and N200 waves were also correlated [Fig. 8(d)]. These group-level data provide further evidence that EROS may be considered as an optical analog of the ERP with the advantage of being a much more localized signal.

Involvement of the prefrontal cortex (PFC) at the early phases (~ 200 ms) of object recognition is debatable. One common view is represented by a feed-forward or bottom-up framework. It has been developed starting from the classical work by Hubel and Wiesel⁴⁰ and puts a lot of emphasis on serial processing within the ventral visual processing route leading from the primary visual cortex to the inferior temporal cortex (IT), where high-level feature neurons (image detectors) are presumably located (for review, see Ref. 41). However, there is growing evidence on the involvement of top-down processes from the PFC that presumably “guide” target feature selection and evaluation. Given a high speed of visual processing, a challenging question is how quickly a top-down process can be initiated. A conceptual model by Bar⁴¹ and supporting experimental data from the same group⁴² have recently suggested and demonstrated an involvement of the PFC very early (100 to 200 ms) in the object recognition process. The key suggestion of the model is that the PFC receives partial information about the visual object (presumably, low spatial frequency information) directly from the primary visual cortex through the dorsal magnocellular pathway, which can deliver this information to the PFC very early (before the complete visual information reaches the inferior temporal cortex). This information can then be used to generate guesses about the object, that are conveyed top-down and guide the recognition process that is finalized within the IT.^{41,42} Our results on EROS provide supportive evidence for the early involvement of the PFC during object detection tasks. Moreover, the temporal course and spatial organization of prefrontal activation observed in the current study corresponds well to the magnetoencephalography (MEG) and fMRI data of Bar et al.⁴² Indeed, the chain of events during recognition of visual objects in the study of Bar et al. started with an initial engagement of the right PFC (early activation at 100 ms in the right frontal eye field; see supplementary Fig. 9 in Ref. 42). Then activation of the left orbitofrontal cortex was observed at 130 ms, followed by activation of the right and left fusiform gyri (IT) at 180 to 215 ms. The left orbitofrontal cortex has been suggested by the authors as being the primary source of top-down control onto the ascending visual processing route. The current study reveals a similar sequence of events (delayed by only ~ 40 ms and somewhat slower), starting with activation of the right middle frontal cortex at 140 ms followed by a peak of activation in the left inferior frontal gyrus at 230 to 250 ms (Fig. 9). The slower time course of events may be due to more complex visual stimuli (natural scenes with a lot of clutter versus line drawings of objects used by Bar et al.⁴²). It is intriguing that the current study also revealed the greatest difference between targets and nontargets in the left inferior frontal gyrus. It is tempting to suggest that the left-hemispheric difference in EROS between targets and nontargets reflects activity of the left-hemispheric orbitofrontal source of top-down influences.⁴²

5 Conclusions

Our results demonstrate reliability of fast optical signals recorded noninvasively as well as their close relationship with EEG and ERP. To successfully record EROS, several guidelines can be suggested: (1) the use of effective algorithms for artifact removal such as ICA; (2) the use of optical probes with linear sizes of at least several cm; (3) bilateral recording; (4) several hundred trials for each experimental condition; (5) if possible, combining FOS recording with EEG. Compared to the ERP, fast optical signals are highly localized and therefore hold promise to become a useful supplementary tool to other imaging techniques that have lower spatial resolution (e.g., EEG). Our data on the early involvement of prefrontal cortex in the Go-NoGo task provide support for the conceptual model, which suggests that the prefrontal cortex is engaged early during object recognition and may facilitate rapid recognition of visual objects by providing top-down influences to the higher centers of the visual system. Overall, fast optical signals can provide a sensitive measure of brain activation with high temporal and spatial resolution, which may be used for more accurate lateralization and cortical mapping of brain processes in a variety of basic research and clinical applications.

Acknowledgments

This work was supported by the NIH (Grant No. R01EB006589 to A.M.), DARPA (Grant No. HB1582-05-C-0045 to J.V.), and The Nancy Lurie Marks Family Foundation. The work was also partially funded by the Intramural Research Program of the Eunice Kennedy Shriver National Institute of Child Health and Human Development at the National Institutes of Health.

References

- D. K. Hill and R. Keynes, "Opacity changes in stimulated nerve," *J. Physiol.* **108**, 278–281 (1945).
- P. Lipton, "Effects of membrane depolarization on light scattering by cerebral cortical slices," *J. Physiol.* **231**(2), 365–383 (1973).
- B. A. MacVicar and D. Hochman, "Imaging of synaptically evoked intrinsic optical signals in hippocampal slices," *J. Neurosci.* **11**(5), 1458–1469 (1991).
- F. F. Jobsis, "Intracellular metabolism of oxygen," *Am. Rev. Respir. Dis.* **110**(6 Pt 2), 58–63 (1974).
- D. M. Rector, G. R. Poe, M. P. Kristensen, and R. M. Harper, "Light scattering changes follow evoked potentials from hippocampal Schaeffer collateral stimulation," *J. Neurophysiol.* **78**(3), 1707–1713 (1997).
- A. Villringer, J. Planck, C. Hock, L. Schleinkofer, and U. Dirnagl, "Near infrared spectroscopy (NIRS): a new tool to study hemodynamic changes during activation of brain function in human adults," *Neurosci. Lett.* **154**(1–2), 101–104 (1993).
- T. Kato, A. Kamei, S. Takashima, and T. Ozaki, "Human visual cortical function during photic stimulation monitoring by means of near-infrared spectroscopy," *J. Cereb. Blood Flow Metab.* **13**(3), 516–520 (1993).
- Y. Hoshi and M. Tamura, "Dynamic multichannel near-infrared optical imaging of human brain activity," *J. Appl. Physiol.* **75**(4), 1842–1846 (1993).
- B. Chance, Z. Zhuang, C. UnAh, C. Alter, and L. Lipton, "Cognition-activated low-frequency modulation of light absorption in human brain," *Proc. Natl. Acad. Sci. USA* **90**(8), 3770–3774 (1993).
- G. Gratton, P. M. Corballis, E. Cho, M. Fabiani, and D. C. Hood, "Shades of gray matter: noninvasive optical images of human brain responses during visual stimulation," *Psychophysiology* **32**(5), 505–509 (1995).
- M. A. Franceschini, S. Fantini, J. H. Thompson, J. P. Culver, and D. A. Boas, "Hemodynamic evoked response of the sensorimotor cortex measured noninvasively with near-infrared optical imaging," *Psychophysiology* **40**(4), 548–560 (2003).
- M. A. Franceschini and D. A. Boas, "Noninvasive measurement of neuronal activity with near-infrared optical imaging," *Neuroimage* **21**(1), 372–386 (2004).
- V. Toronov, M. A. Franceschini, M. Filiaci, S. Fantini, M. Wolf, A. Michalos, and E. Gratton, "Near-infrared study of fluctuations in cerebral hemodynamics during rest and motor stimulation: temporal analysis and spatial mapping," *Med. Phys.* **27**(4), 801–815 (2000).
- V. Toronov, A. Webb, J. H. Choi, M. Wolf, A. Michalos, E. Gratton, and D. Hueber, "Investigation of human brain hemodynamics by simultaneous near-infrared spectroscopy and functional magnetic resonance imaging," *Med. Phys.* **28**(4), 521–527 (2001).
- G. Gratton, M. Fabiani, P. M. Corballis, D. C. Hood, M. R. Goodman-Wood, J. Hirsch, K. Kim, D. Friedman, and E. Gratton, "Fast and localized event-related optical signals (EROS) in the human occipital cortex: comparisons with the visual evoked potential and fMRI," *Neuroimage* **6**(3), 168–180 (1997).
- T. Rinne, G. Gratton, M. Fabiani, N. Cowan, E. Maclin, A. Stinard, J. Sinkkonen, K. Alho, and R. Naatanen, "Scalp-recorded optical signals make sound processing in the auditory cortex visible?" *Neuroimage* **10**(5), 620–624 (1999).
- J. Steinbrink, M. Kohl, H. Obrig, G. Curio, F. Syre, F. Thomas, H. Wabnitz, H. Rinneberg, and A. Villringer, "Somatosensory evoked fast optical intensity changes detected non-invasively in the adult human head," *Neurosci. Lett.* **291**(2), 105–108 (2000).
- M. Wolf, U. Wolf, J. H. Choi, R. Gupta, L. P. Safanova, L. A. Paunesku, A. Michalos, and E. Gratton, "Functional frequency-domain near-infrared spectroscopy detects fast neuronal signal in the motor cortex," *Neuroimage* **17**(4), 1868–1875 (2002).
- F. Syre, H. Obrig, J. Steinbrink, M. Kohl, R. Wenzel, and A. Villringer, "Are VEP correlated fast optical signals detectable in the human adult by non-invasive nearinfrared spectroscopy (NIRS)?" *Adv. Exp. Med. Biol.* **530**, 421–431 (2003).
- G. Gratton and M. Fabiani, "The event-related optical signal (EROS) in visual cortex: replicability, consistency, localization, and resolution," *Psychophysiology* **40**(4), 561–571 (2003).
- M. Wolf, U. Wolf, J. H. Choi, V. Toronov, L. A. Paunesku, A. Michalos, and E. Gratton, "Fast cerebral functional signal in the 100-ms range detected in the visual cortex by frequency-domain near-infrared spectrophotometry," *Psychophysiology* **40**(4), 521–528 (2003).
- G. Morren, U. Wolf, P. Lemmerling, M. Wolf, J. H. Choi, E. Gratton, L. De Lathauwer, and S. Van Huffel, "Detection of fast neuronal signals in the motor cortex from functional near infrared spectroscopy measurements using independent component analysis," *Med. Biol. Eng. Comput.* **42**(1), 92–99 (2004).
- J. Steinbrink, F. C. Kempf, A. Villringer, and H. Obrig, "The fast optical signal—robust or elusive when non-invasively measured in the human adult?" *Neuroimage* **26**(4), 996–1008 (2005).
- E. L. Maclin, K. A. Low, J. J. Sable, M. Fabiani, and G. Gratton, "The event-related optical signal to electrical stimulation of the median nerve," *Neuroimage* **21**(4), 1798–1804 (2004).
- H. Radhakrishnan, W. Vanduffel, H. P. Deng, L. Ekstrom, D. A. Boas, and M. A. Franceschini, "Fast optical signal not detected in awake behaving monkeys," *Neuroimage* **45**(2), 410–419 (2009).
- A. Pfefferbaum, J. M. Ford, B. J. Weller, and B. S. Kopell, "ERPs to response production and inhibition," *Electroencephalogr. Clin. Neurophysiol.* **60**(5), 423–434 (1985).
- A. Rodriguez-Fornells, B. M. Schmitt, M. Kutas, and T. F. Munte, "Electrophysiological estimates of the time course of semantic and phonological encoding during listening and naming," *Neuropsychologia* **40**(7), 778–787 (2002).
- S. Thorpe, D. Fize, and C. Marlot, "Speed of processing in the human visual system," *Nature* **381**(6582), 520–522 (1996).
- A. V. Medvedev, J. M. Kainerstorfer, S. V. Borisov, and J. VanMeter, "Functional connectivity in the prefrontal cortex measured by near-infrared spectroscopy during ultra-rapid object recognition," *J. Biomed. Opt.* (submitted).
- A. Hyvärinen and E. Oja, "Independent component analysis: algorithms and applications," *Neural Netw.* **13**(4–5), 411–430 (2000).

31. A. Delorme and S. Makeig, "EEGLAB: an open source toolbox for analysis of single-trial EEG dynamics including independent component analysis," *J. Neurosci. Methods* **134**(1), 9–21 (2004).
32. A. V. Medvedev, J. Kainerstorfer, S. V. Borisov, R. L. Barbour, and J. VanMeter, "Event-related fast optical signal in a rapid object recognition task: improving detection by the Independent Component Analysis," *Brain Res.* **1236**, 145–158 (2008); available at <http://dx.doi.org/10.1016/j.brainres.2008.07.122>.
33. P. L. Nunez and R. Srinivasan, *Electric Fields of the Brain: The Neurophysics of EEG*, Oxford University Press, New York (2006).
34. R. A. Stepnoski, A. LaPorta, F. Racchia-Behling, G. E. Blonder, R. E. Slusher, and D. Kleinfeld, "Noninvasive detection of changes in membrane potential in cultured neurons by light scattering," *Proc. Natl. Acad. Sci. USA* **88**(21), 9382–9386 (1991).
35. K. A. Low, E. Leaver, A. F. Kramer, M. Fabiani, and G. Gratton, "Fast optical imaging of frontal cortex during active and passive oddball tasks," *Psychophysiology* **43**(2), 127–136 (2006).
36. G. Strangman, J. P. Culver, J. H. Thompson, and D. A. Boas, "A quantitative comparison of simultaneous BOLD fMRI and NIRS recordings during functional brain activation," *Neuroimage* **17**(2), 719–731 (2002).
37. G. Gratton and P. M. Corballis, "Removing the heart from the brain: compensation for the pulse artifact in the photon migration signal," *Psychophysiology* **32**(3), 292–299 (1995).
38. Q. Zhang, E. N. Brown, and G. E. Strangman, "Adaptive filtering to reduce global interference in evoked brain activity detection: a human subject case study," *J. Biomed. Opt.* **12**(6), 064009 (2007).
39. G. Gratton, C. R. Brumback, B. A. Gordon, M. A. Pearson, K. A. Low, and M. Fabiani, "Effects of measurement method, wavelength, and source-detector distance on the fast optical signal," *Neuroimage* **32**(4), 1576–1590 (2006).
40. D. H. Hubel and T. N. Wiesel, "Receptive fields and functional architecture in two nonstriate visual areas (18 and 19) of the cat," *J. Neurophysiol.* **28**, 229–289 (1965).
41. M. Bar, "A cortical mechanism for triggering top-down facilitation in visual object recognition," *J. Cogn. Neurosci.* **15**(4), 600–609 (2003).
42. M. Bar, K. S. Kassam, A. S. Ghuman, J. Boshyan, A. M. Schmid, A. M. Dale, M. S. Hamalainen, K. Marinkovic, D. L. Schacter, B. R. Rosen, and E. Halgren, "Top-down facilitation of visual recognition," *Proc. Natl. Acad. Sci. USA* **103**(2), 449–454 (2006).